

MN48: a new Galactic bona fide luminous blue variable revealed by *Spitzer* and SALT*

A. Y. Kniazev,^{1,2,3†} V. V. Gvaramadze,^{3,4,5} L. N. Berdnikov^{3,5,6}

¹South African Astronomical Observatory, PO Box 9, 7935 Observatory, Cape Town, South Africa

²Southern African Large Telescope Foundation, PO Box 9, 7935 Observatory, Cape Town, South Africa

³Sternberg Astronomical Institute, Lomonosov Moscow State University, Universitetskij Pr. 13, Moscow 119992, Russia

⁴Space Research Institute, Russian Academy of Sciences, Profsoyuznaya 84/32, Moscow 117997, Russia

⁵Isaac Newton Institute of Chile, Moscow Branch, Universitetskij Pr. 13, Moscow 119992, Russia

⁶Astronomy and Astrophysics Research division, Entoto Observatory and Research Center, PO Box 8412 Addis Ababa, Ethiopia

Accepted 2016 April 13. Received 2016 April 13; in original form 2016 February 7

ABSTRACT

In this paper, we report the results of spectroscopic and photometric observations of the candidate evolved massive star MN48 disclosed via detection of a mid-infrared circular shell around it with the *Spitzer Space Telescope*. Follow-up optical spectroscopy of MN48 with the Southern African Large Telescope (SALT) carried out in 2011–2015 revealed significant changes in the spectrum of this star, which are typical of luminous blue variables (LBVs). The LBV status of MN48 was further supported by photometric monitoring which shows that in 2009–2011 this star has brightened by ≈ 0.9 and 1 mag in the V and I_c bands, respectively, then faded by ≈ 1.1 and 1.6 mag during the next four years, and apparently started to brighten again recently. The detected changes in the spectrum and brightness of MN48 make this star the 18th known Galactic bona fide LBV and increase the percentage of LBVs associated with circumstellar nebulae to more than 70 per cent. We discuss the possible birth place of MN48 and suggest that this star might have been ejected either from a putative star cluster embedded in the H II region IRAS 16455–4531 or the young massive star cluster Westerlund 1.

Key words: line: identification – circumstellar matter – stars: emission-line, Be – stars: evolution – stars: individual: [GKF2010]MN48 – stars: massive.

1 INTRODUCTION

Luminous blue variables (LBVs) belong to a very rare class of massive stars at advanced evolutionary stages (Conti 1984), characterized by spectacular photometric and spectral variability (Humphreys & Davidson 1994; van Genderen 2001). During major eruptions, LBVs can be confused with supernovae (e.g. Goodrich et al. 1989; Filippenko et al. 1995). The nature of the LBV phenomenon as well as the evolutionary status of LBVs remain unclear. Although it is believed that the LBV phase is intermediate between the main sequence and Wolf-Rayet phases (e.g. Langer et al. 1994; Stothers & Chin 1996), there are strong indications that some LBVs are immediate precursors of supernovae

(e.g. Kotak & Vink 2006; Gal-Yam & Leonard 2009; Groh, Meynet & Ekström 2013; Groh et al. 2013). Revealing of new examples of LBVs might be of crucial importance for understanding these enigmatic objects.

The majority (≈ 70 per cent; Kniazev, Gvaramadze & Berdnikov 2015) of the LBVs are surrounded by compact (circular or bipolar) circumstellar nebulae, composed of stellar material ejected during the LBV and/or preceding evolutionary stages (Nota et al. 1995). Detection of such nebulae serves as an indication that their underlying stars are LBVs or related evolved massive stars. Subsequent searches for significant changes in the brightness and spectra of these stars are necessary to determine which of them are bona fide LBVs.

Until recently, only three LBV candidates were revealed through the detection of (mid-infrared) circumstellar shells and follow-up spectroscopy of their central stars (Waters et al. 1996; Egan et al. 2002; Clark et al. 2003). This is mostly because of low angular resolution and sensitivity of the data (obtained with the *InfraRed Astronomical Satellite*

* Based on observations obtained with the Southern African Large Telescope (SALT), programmes 2010-1-RSA_OTH-001, 2013-1-RSA_OTH-014 and 2013-2-RSA_OTH-003 (PI: A. Y. Kniazev).

† E-mail: akniazev@sao.ac.za

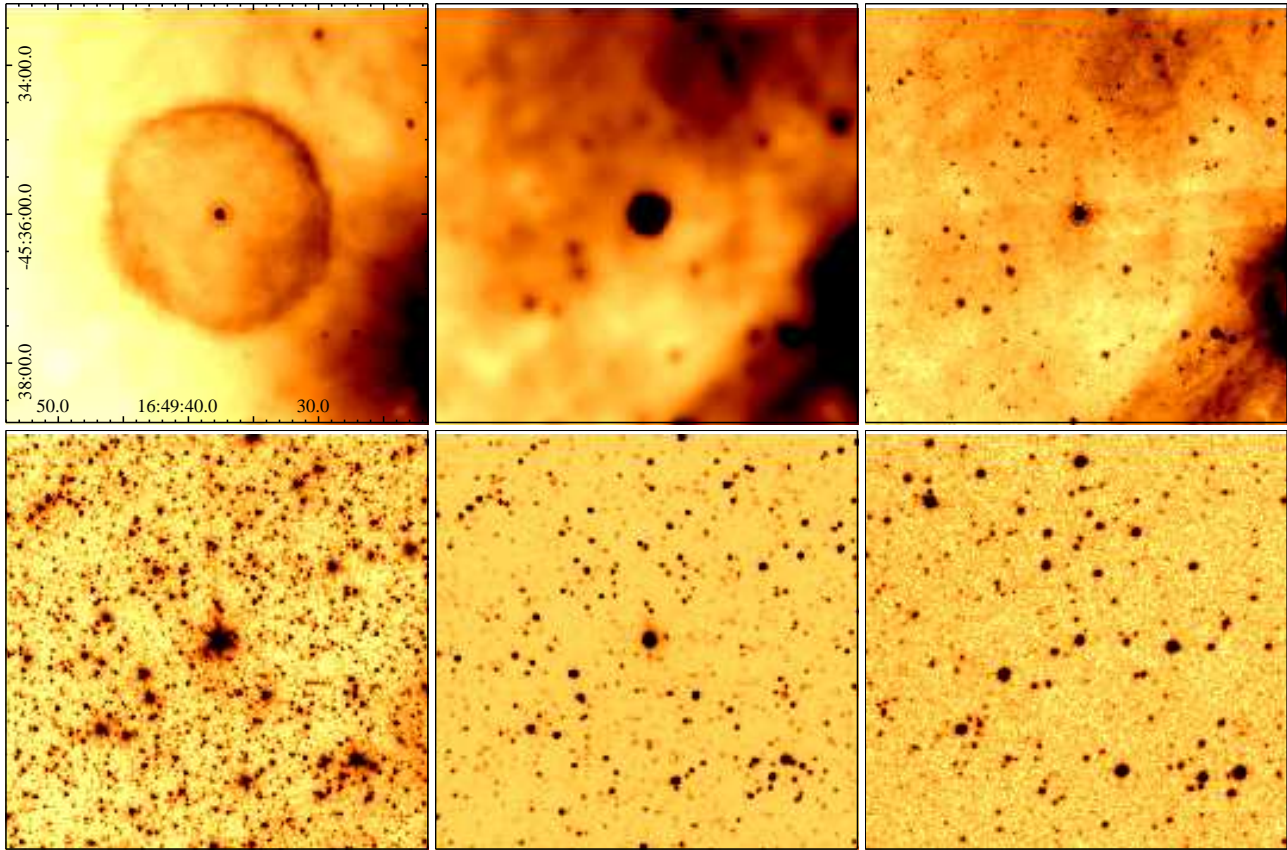


Figure 1. From left to right, and from top to bottom: *Spitzer* MIPS $24\ \mu\text{m}$, *WISE* $12\ \mu\text{m}$, IRAC 8 and $3.6\ \mu\text{m}$, 2MASS K_s band and DSS II red band images of the region containing the nebula MN48 and its central star (the scale of the images is the same). A bright emission to the south-west of MN48 is the H II region IRAS 16455–4531. The coordinates are in units of RA (J2000) and Dec. (J2000) on the horizontal and vertical scales, respectively.

and the *Midcourse Space Experiment* satellite) being used. The situation has been improved drastically with the advent of the *Spitzer Space Telescope*. Searches for compact nebulae using the *Spitzer* data resulted in discovery of many dozens of compact nebulae, whose geometry is reminiscent of that of the nebulae associated with the already known LBVs (Gvaramadze, Kniazev & Fabrika 2010b; Wachter et al. 2010; Mizuno et al. 2010). Spectroscopy of central stars of these nebulae showed that many of them have spectra similar to those of the LBVs, which further supports the LBV nature of these stars (Gvaramadze et al. 2010a,b, 2015a; Wachter et al. 2010, 2011; Stringfellow et al. 2012a,b; Flagey et al. 2014; Kniazev & Gvaramadze 2016).

The majority of the compact nebulae discovered with *Spitzer* were detected in $24\ \mu\text{m}$ images obtained with the Multiband Imaging Photometer for *Spitzer* (MIPS; Rieke et al. 2004) within the framework of the 24 and 70 Micron Survey of the Inner Galactic Disk with MIPS (MIPSGAL; Carey et al. 2009) and other *Spitzer* programmes¹. Some of them have obvious counterparts at shorter wavelengths and can be detected at 8, 5.8, 4.5 and $3.6\ \mu\text{m}$ images obtained with the *Spitzer* Infrared Array Camera (IRAC; Fazio et al. 2004). In some cases, the nebulae were discovered us-

ing the IRAC data only because the corresponding MIPS images are oversaturated (Gvaramadze et al. 2010b). The number of new detections of compact nebulae continues to increase (Gvaramadze et al. 2011, 2012a; Kniazev & Gvaramadze 2016) with the release of an all-sky survey in 3.4, 4.6, 12 and $22\ \mu\text{m}$ bands performed with the *Wide-field Infrared Survey Explorer* (*WISE*; Wright et al. 2010). This, in turn, leads to further increase of the number of newly identified LBV candidates (Gvaramadze et al. 2012a; Kniazev & Gvaramadze 2016).

In 2009 we started a monitoring campaign of LBV candidates revealed with *Spitzer* (and later on with *WISE*) in order to search for their possible spectral and photometric variability, and potentially to prove that at least some of them are bona fide LBVs. Since then, we have confirmed the LBV status of three of these stars: Wray 16-137 (Gvaramadze et al. 2014), WS1 (Kniazev, Gvaramadze & Berdnikov 2015) and MN44 (Gvaramadze, Kniazev & Berdnikov 2015b). In this paper, we present observations indicating that a fourth star in our sample, MN48, is a bona fide LBV as well. In Section 2, we present the star and its nebula. In Section 3, we describe our spectroscopic and photometric observations. The results are discussed in Section 4.

¹ <http://irsa.ipac.caltech.edu/Missions/spitzer.html>

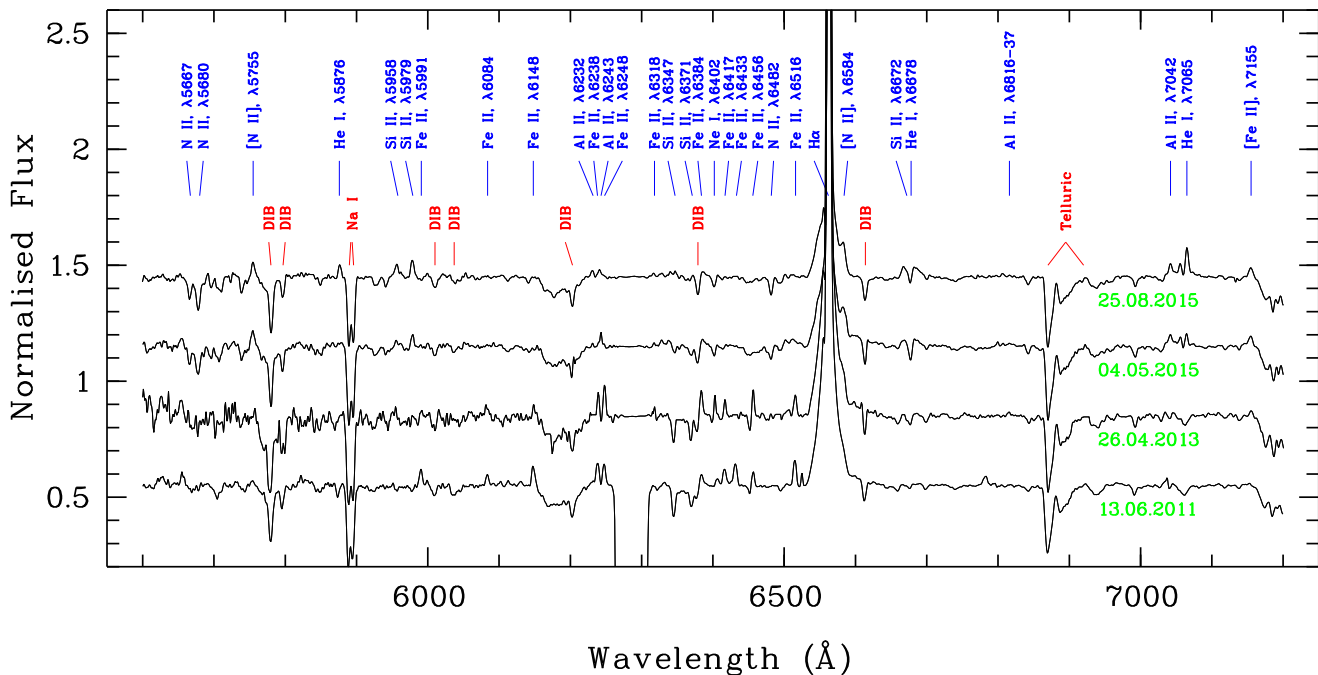


Figure 2. Evolution of the (normalized) long-slit spectrum of MN48 in 2011–2015. Principal lines and most prominent DIBs are indicated.

2 MN48 AND ITS MID-INFRARED NEBULA

The nebula around MN48 was discovered in Gvaramadze et al. (2010b; see their fig.1i) using the data of the *Spitzer*/MIPSGAL survey (Carey et al. 2009). In the Set of Identifications, Measurements and Bibliography for Astronomical Data (SIMBAD) data base², this nebula is named [GKF2010] MN48. Like the majority of other mid-infrared nebulae discovered with *Spitzer* and *WISE*, the nebula around MN48 emerges in all its glory only in the *Spitzer* 24 μm and *WISE* 22 μm images³. At 24 μm it appears (see the upper, left-hand panel of Fig.1) as a nearly circular (slightly elongated southwest to northeast) shell of radius of ≈ 1.5 arcmin⁴, with a rather ragged rim. There are also some hints of 12 and 8 μm emission (more obvious at 12 μm) probably associated with the western (more bright) edge of the nebula (see the upper, middle and right-hand panels of Fig.1). The enhanced brightness of this part of the nebula might be caused by the interaction of the nebula with the H II region IRAS 16455–4531, which is located at ≈ 5 arcmin to the west (the possible association between MN48 and IRAS 16455–4531 is discussed in Section 4.3).

MN48 is prominent at 24 μm , in all IRAC and *WISE*

Table 1. Journal of the long-slit observations.

Date	Exposure (min)	Slit/Seeing (arcsec)	JD (d)
2011 June 13	1×10	1.00/1.8	2455725
2013 April 26	1×10	1.25/1.5	2456408
2015 May 4	1×10	1.25/0.9	2457146
2015 August 25	1×15	1.25/1.4	2457259

wavebands, and in all (*J*, *H*, *K_s*) Two-Micron All Sky Survey (2MASS) images (Skrutskie et al., 2006). The 2MASS coordinates of this star are: $\alpha_{2000} = 16^{\text{h}}49^{\text{m}}37^{\text{s}}.70$, $\delta_{J2000} = -45^{\circ}35'59''.3$ and $l = 340^{\circ}0298$, $b = -0^{\circ}5839$. More importantly, MN48 is also visible in the optical wavebands [see the lower, right-hand panel of Fig.1 for the Digitized Sky Survey II (DSS-II) red band (McLean et al. 2000) image], which makes this star a good target for our observing programmes with the Southern African Large Telescope (SALT).

Wachter et al. (2010, 2011) classified MN48 (or star #20 in their designation) as a Be star by means of infrared spectroscopy. The *H* and *K* band spectra of this star were presented in fig. 6 of Wachter et al. (2010).

3 OBSERVATIONS OF MN48

3.1 Long-slit SALT spectroscopy

MN48 was observed with the SALT (Buckley, Swart & Meiring 2006; O’Donoghue et al. 2006) on four occasions in 2011–2015 (see Table 1 for the log of the observations). The spectra were taken with the Robert Stobie Spectrograph (RSS;

² <http://simbad.harvard.edu/simbad/>

³ *Spitzer* spectroscopy of circumstellar nebulae around evolved massive stars showed that their emission is dominated by the dust continuum emission (Flagey et al. 2011; Nowak et al. 2014). Detection of the nebula around MN48 at longer wavelengths (e.g. in the *Herschel* data or with the APEX/LABOCA) could, therefore, be used to estimate its mass and to constrain the mass-loss history of the star itself.

⁴ The angular size of the nebula around MN48 is the largest among 115 nebulae discovered in Gvaramadze et al. (2010b).

Table 2. EWs, FWHMs and RVs of some lines in the spectra of MN48.

λ_0 (Å) Ion	EW(λ) (Å)	FWHM(λ) (Å)	RV (km s^{-1})
2011 June 13			
6347 Si II	-0.73 ± 0.05	6.05 ± 0.33	-95 ± 19
6563 H α	28.58 ± 0.90	6.85 ± 0.25	-21 ± 18
2013 April 26			
6347 Si II	-0.48 ± 0.06	5.04 ± 0.19	-100 ± 15
6563 H α	47.05 ± 0.88	5.44 ± 0.12	8 ± 15
7155 [Fe II]	0.08 ± 0.05	4.12 ± 0.54	7 ± 16
2015 May 4			
4861 H β	2.91 ± 0.19	6.98 ± 0.54	75 ± 15
5755 [N II]	0.30 ± 0.05	5.33 ± 0.40	7 ± 10
6347 Si II	-0.10 ± 0.04	3.95 ± 0.72	-27 ± 12
6563 H α	22.21 ± 0.55	5.19 ± 0.15	24 ± 15
7065 He I	0.26 ± 0.05	4.18 ± 0.24	-19 ± 18
7155 [Fe II]	0.20 ± 0.05	6.75 ± 0.34	-33 ± 15
2015 August 25			
4861 H β	3.93 ± 0.29	4.88 ± 0.41	-32 ± 12
5755 [N II]	0.29 ± 0.02	4.87 ± 0.28	-9 ± 8
5876 He I	0.23 ± 0.02	4.12 ± 0.30	20 ± 8
6347 Si II	0.02 ± 0.01	4.69 ± 0.37	-29 ± 7
6563 H α	20.84 ± 0.47	5.41 ± 0.14	0 ± 5
7065 He I	0.61 ± 0.03	5.48 ± 0.24	-32 ± 6
7155 [Fe II]	0.23 ± 0.02	5.82 ± 0.44	-54 ± 9
2015 August 26 (échelle)			
6563 H α	20.21 ± 0.12	1.57 ± 0.02	-11.4 ± 0.4
6584 [N II]	0.43 ± 0.02	5.29 ± 0.17	-28.2 ± 3.3
7065 He I	0.60 ± 0.01	2.17 ± 0.06	-38.2 ± 1.1
7772 O I	-0.64 ± 0.01	2.69 ± 0.03	-43.4 ± 0.3
7774 O I	-0.41 ± 0.01	1.61 ± 0.04	-29.3 ± 0.3
7775 O I	-0.05 ± 0.01	0.72 ± 0.05	-28.4 ± 0.3
7877 Mg II	0.50 ± 0.01	1.57 ± 0.03	-45.5 ± 0.5
7896 Mg II	0.61 ± 0.01	1.74 ± 0.02	-43.7 ± 0.4

Note: The negative EWs correspond to absorption lines.

Burgh et al. 2003; Kobulnicky et al. 2003) in the long-slit mode. The PG900 grating was used for all observations, and in all cases the spectral range of 4200 – 7300 Å was covered with a final reciprocal dispersion of 0.97 Å pixel⁻¹. The spectral resolution full width at half-maximum (FWHM) was of 4.40±0.15 Å. Because the spectra were taken during bright time, their blue parts (shortward of ≈5600 Å) are very noisy and do not contain meaningful information. A Xe lamp arc spectrum was taken immediately after all science frames. Spectrophotometric standard stars were observed during twilight time for relative flux calibration. Absolute flux calibration is not feasible with SALT because the unfilled entrance pupil of the telescope moves during the observations.

Primary reduction of the data was done in the standard way with the SALT science pipeline (Crawford et al. 2010). Following long-slit data reduction was carried out in the way described in Kniazev et al. (2008). The resulting normalized spectra are presented in Fig. 2. The principal lines and most prominent diffuse interstellar bands (DIBs) are in-

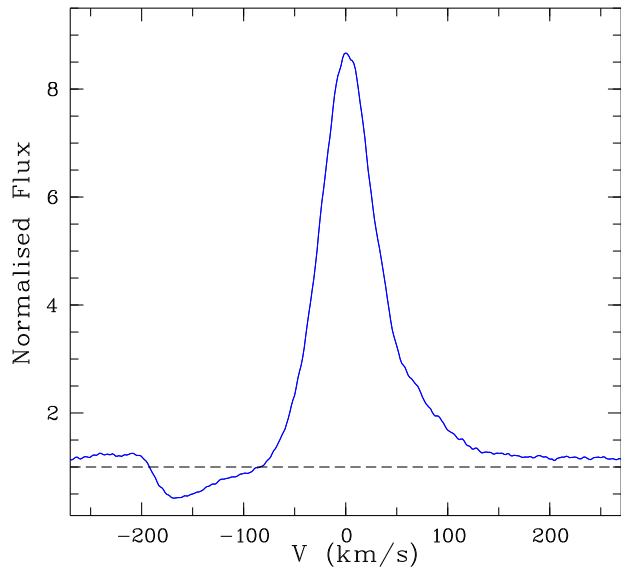


Figure 3. The H α line profile in the échelle spectrum. The blue edge of the absorption component corresponds to the terminal wind velocity of $\approx 200 \text{ km s}^{-1}$.

dicated. All wavelengths are given in air. Equivalent widths (EWs), FWHMs and heliocentric radial velocities (RVs) of some lines in the spectra (measured applying the MIDAS programs; see Kniazev et al. 2004 for details) are given in Table 2.

3.2 Échelle spectroscopy with the SALT

MN48 was also observed with the SALT High Resolution Spectrograph (HRS; Barnes et al. 2008; Bramall et al. 2010, 2012; Crause et al. 2014) on 2015 August 26 with a single exposure of 1800 s and seeing of about 3 arcsec. The HRS is a dual beam, fibre-fed échelle spectrograph. It was used in the low resolution mode ($R \sim 14000$ and 2.23 arcsec diameter for both the object and sky fibers) to provide a spectrum in the blue and red arms over the total spectral range of ≈ 3700 – 8900 Å. The both blue and red arms CCD were read out by a single amplifier with a 1×1 binning. Three arc spectra of ThAr+Ar lamps and three spectral flats were obtained in this mode during a weekly set of HRS calibrations. MN48 is a highly reddened object and for this reason the blue arm spectrum is unusable. The red arm spectrum has a signal-to-noise ratio per pixel of ≥ 25 in the middle of spectral orders starting from ~ 6300 Å and could be used for the brightest longward lines. Because of problems with the CCD in the red arm science frame, however, a part of the spectrum beyond ≈ 8500 Å was unusable for analysis.

Primary reduction of the HRS data, including overscan correction, bias subtractions and gain correction, was done with the SALT science pipeline (Crawford et al. 2010). Spectroscopic reduction of the red arm data was carried out using standard MIDAS *feros* (Stahl, Kaufer & Tubbesing 1999) and *echelle* (Ballester 1992) packages. We have performed the following steps: (1) positions for 33 spectral orders (from 53 till 85) for both fibers were found using spectral flats frames; (2) the 2D background was determined and sub-

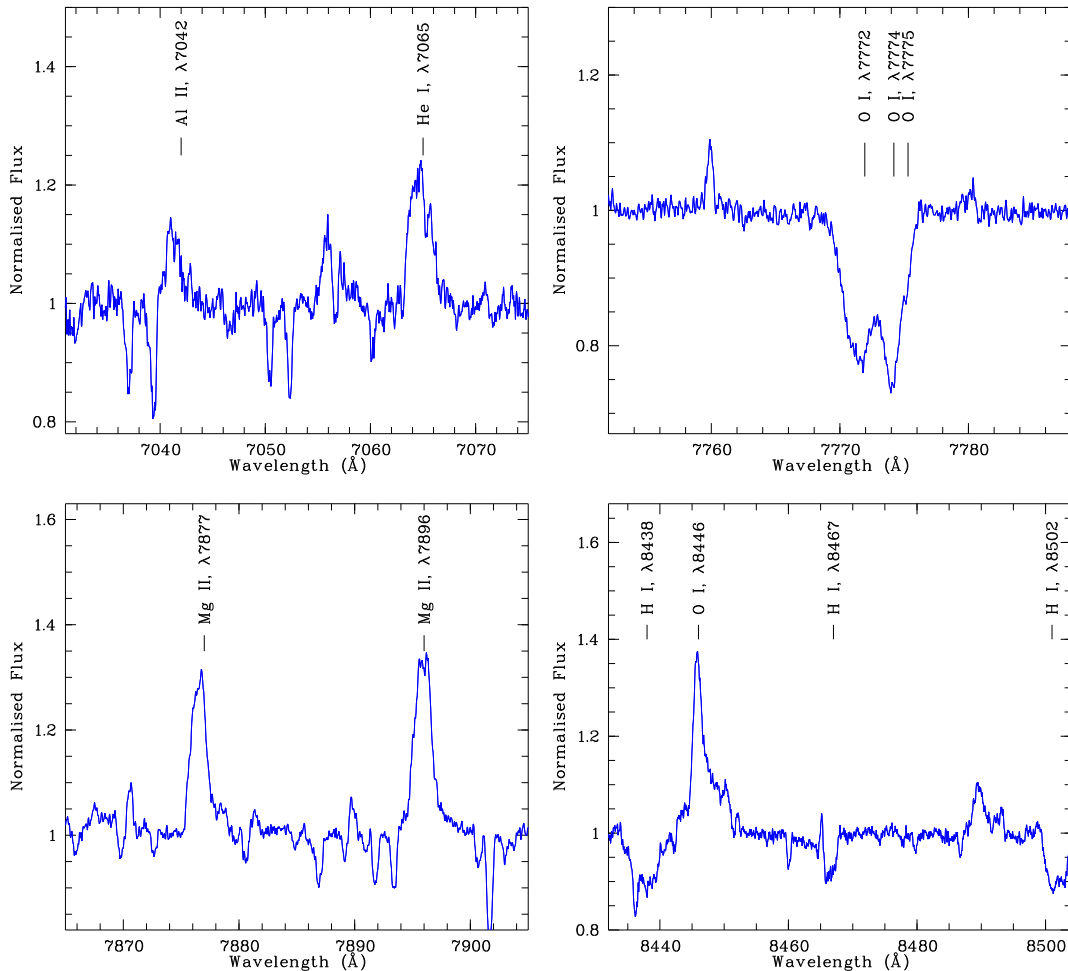


Figure 4. Portions of the échelle spectrum of MN48 (obtained on 2015 August 26). Narrow unlabeled absorption lines (e.g. at 7037, 7040, 7049 and 7051 Å) are telluric in origin.

tracted from all frames; (3) the straightened échelle spectrum was extracted for both fibers from all types of frames (flats, arcs and object) using the standard mode with cosmic masking and the optimum extraction algorithms; (4) for the object and sky fibers the blaze function was removed from the science frame through division to extracted spectrum of spectral flat; (5) the procedure found ~ 1100 emission lines in the extracted arc spectrum of which ~ 450 lines were finally automatically identified with requested level of tolerance to build a 2D dispersion curve with the final mean rms of 0.006 \AA (this step was done independently for the object and sky fibers); (6) all extracted orders were rebinned into linear wavelength steps and the wavelength calibrated sky fiber orders were subtracted from the object fiber orders; (7) all orders for the object fiber were merged into a 1D file. The total spectral range of $5400\text{--}8500 \text{ \AA}$ was covered with a final reciprocal dispersion of $0.04 \text{ \AA pixel}^{-1}$. The spectral resolution FWHM (measured using wavelength calibrated arc spectrum) changes from $\approx 0.34 \text{ \AA}$ in the blue part of the spectrum ($R \sim 16500$) to $\approx 0.57 \text{ \AA}$ in the red part ($R \sim 15500$).

EWs, FWHMs and RVs of some lines in the HRS spectrum are given in Table 2. We estimated the accuracy of the continuum normalization to be better than 5 per cent. The

comparison of the EWs of the $H\alpha$ line in the RSS and HRS spectra obtained during two sequential nights supports this estimate. Several portions of the échelle spectrum (not corrected for barycentric motion) are presented in Figs 3 and 4. Fig. 3 shows that the $H\alpha$ line has a clear P Cygni profile. Note that the line profiles of the Paschen lines seen in the lower right panel of Fig. 4 are quite different from those observed in the spectra of the classical LBVs like P Cygni (Stahl et al. 1993) and AG Car (Groh et al. 2009). Better observational data are required to check whether this distinction is real or is due to instrumental effects.

3.3 Photometry

To search for photometric variability of MN48, we occasionally obtained its CCD photometry with the 40-cm telescope of the Observatorio Cerro Armazones (OCA) of the North Catholic University (Chile) and the 76-cm telescope of the South African Astronomical Observatory during our observing runs in 2009–2014. We used an SBIG ST-10XME CCD camera equipped with BVI_c filters of the Kron-Cousins system (for details see Berdnikov et al. 2012) to build the system of secondary standards in the field of MN48. With these

Table 3. Archival and contemporary photometry of MN48.

Date	<i>B</i>	<i>V</i>	<i>I_c</i>	<i>V</i> − <i>I_c</i>	<i>J</i>	<i>K</i>	JD
1976 April 30 ^a	18.6±0.3	–	–	–	–	–	244 2899
1980 July 22 ^a	–	–	11.20±0.20	–	–	–	244 4442
1998 July 28 ^b	–	–	10.82±0.02	–	7.87±0.10	4.54±0.12	245 1023
1999 May 23 ^c	–	–	–	–	7.24±0.02	5.42±0.02	245 1322
1999 June 25 ^b	–	–	11.07±0.03	–	7.11±0.10	4.86±0.09	245 1355
2009 April 18 ^d	–	16.05±0.05	10.74±0.02	5.31±0.05	–	–	245 4940
2011 May 10 ^e	18.18±0.10	15.19±0.03	9.73±0.01	5.46±0.03	–	–	245 5692
2012 May 6 ^e	–	15.26±0.01	9.93±0.01	5.33±0.02	–	–	245 6054
2013 January 24 ^e	–	15.61±0.02	10.29±0.01	5.32±0.02	–	–	245 6316
2014 April 25 ^e	19.27±0.20	15.92±0.05	10.69±0.04	5.23±0.06	–	–	245 6772
2015 May 4 ^f	–	–	11.26±0.08	–	–	–	245 7146
2015 May 19 ^g	–	16.33±0.03	11.19±0.04	5.14±0.05	–	–	245 7161
2015 August 25 ^f	–	–	11.33±0.06	–	–	–	245 7259
2016 February 2 ^h	–	16.24±0.03	11.10±0.03	5.14±0.04	–	–	245 7420

^aUSNO B-1; ^bDENIS; ^c2MASS; ^d40-cm telescope; ^e76-cm telescope; ^fSALT; ^g1-m telescope; ^hLCOGT.

standards, we derived *V* and *I_c* magnitudes of MN48 using images obtained with the SAAO 1-m telescope on 2015 May 19, an *I_c* magnitude using acquisition images obtained with the SALT on 2015 May 4 and August 25, and *V* and *I_c* magnitudes from images obtained with the Las Cumbres Observatory Global Telescope (LCOGT) network (Brown et al. 2013) on 2016 February 2. Using the same standards, we recalibrated the *I* and *B* magnitudes from the USNO B-1 catalogue (Monet et al. 2003). The results are presented in Table 3. To this table we also added the *J* and *K_s* magnitudes from 2MASS (Cutri et al. 2003) and two-epoch *I*, *J* and *K* photometry from the Deep Near Infrared Survey of the Southern Sky (DENIS; Epchtein et al. 1999).

The *V* and *I* band light curves of MN48, based on our observations in 2009–2016, are presented in Fig. 5. The arrows indicate times when the spectra were obtained with the SALT. For each data point (square) we give 1 σ error bars, which in most cases are less than the size of the squares themselves and therefore they cannot be discerned.

4 DISCUSSION

4.1 MN48: a new Galactic bona fide LBV

Inspection of Table 3 and Fig. 5 shows that MN48 has brightened in the *V* and *I_c* bands, respectively, by ≈ 0.9 and 1 mag during the first two years of our photometric monitoring campaign and reached the maximum light by the time of our first spectroscopic observation in 2011. Since then, MN48 started to fade and its brightness in the *V* and *I_c* bands has dropped, respectively, by ≈ 1.1 and 1.6 mag during the next four years. The last data points (obtained on 2016 February 2) suggest that MN48 has started to brighten again.

The photometric variability of MN48 could also be inferred from comparison of the *I_c* magnitudes based on our observations with those given in the USNO B-1 and DENIS catalogues, as well as from comparison of the two epoch DENIS *J* and *K* photometry with the 2MASS photometry (see Table 3). Interestingly, while the *J* band brightness of MN48 increased by ≈ 0.8 mag during ≈ 11 months in 1998–1999, the *K* band brightness instead faded by ≈ 0.9 mag during

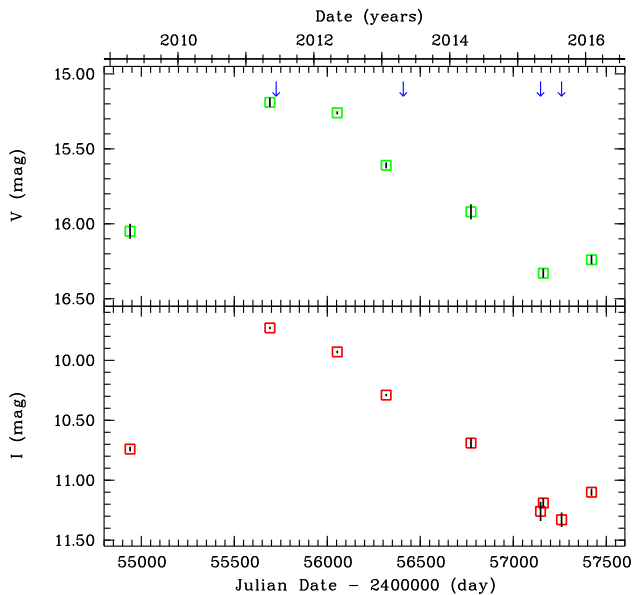


Figure 5. Light curves of MN48 in the *V* and *I* bands in 2009–2016. 1 σ error bars are indicated, but in most cases they are within the size of the data points (boxes). The arrows mark the dates of the SALT spectra.

the first 10 months and then increased by ≈ 0.6 mag during the next month. Also, comparison of the IRAC 4.5 μm magnitude of MN48 of 5.02 ± 0.06 (Spitzer Science Center 2009) with the *WISE* 4.6 μm magnitude of 3.63 ± 0.14 (Cutri et al. 2014) indicates that the star became brighter by a factor of about 3 on a time scale of four years.

From Table 3 also follows that the *V* − *I_c* colour of MN48 has increased (i.e. the star became redder) with the brightness increase and then started to decrease with the brightness decline (i.e. the star becomes bluer). These changes in the colour (see Fig. 6) suggest that the effective temperature, T_{eff} , of MN48 has decreased during the first two years of our photometric observations and after reaching the minimum value by 2011 June has started to increase (e.g. van Genderen 1982). This behaviour is typical of LBVs experi-

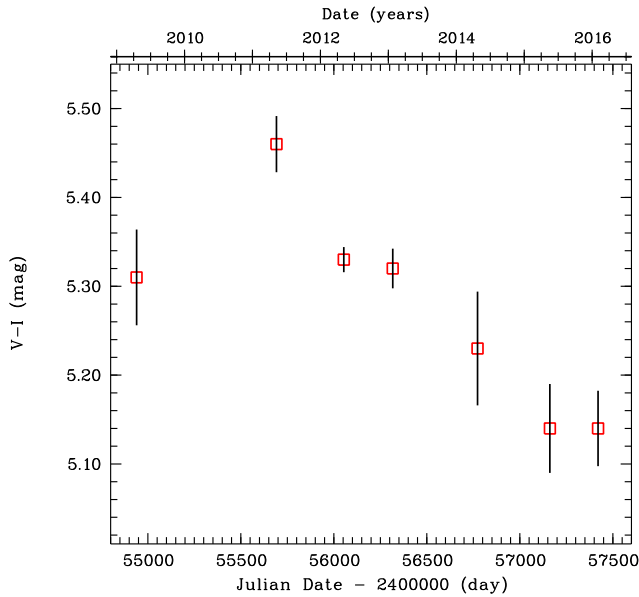


Figure 6. Evolution of the $V-I_c$ colour of MN48 with time.

encing S Dor-like outbursts and it should be accompanied by noticeable changes in the spectral appearance of the star (e.g. Stahl et al. 2001).

Indeed, inspection of the RSS spectra presented in Fig. 2 confirms that MN48 became hotter during the last four years, which is manifested in the almost complete disappearance of the Fe II lines in the 2015's spectra (cf. Stahl et al. 2001) and significant changes in the temperature sensitive lines like N II $\lambda\lambda$ 5667, 5680, 6482, Si II $\lambda\lambda$ 6347, 6371, and Ne II λ 6402 (e.g. Walborn 1980; Lennon, Dufton & Fitzsimmons 1993). Particularly, the Si II $\lambda\lambda$ 6347, 6371 doublet was very prominent in 2011 and 2013 and is hardly visible in 2015, which implies that T_{eff} of MN48 has increased by several thousand degrees during the last two years (e.g. Lennon et al. 1993).

The brightness decline of MN48 is accompanied by appearance of forbidden lines of [N II] $\lambda\lambda$ 5755, 6584 and [Fe II] λ 7155, which became prominent in the 2015's spectra. The spectra also show significant changes in the profiles of the He I $\lambda\lambda$ 6676, 7065 lines. These lines were weakly in absorption in the 2011's spectrum, but increased their strength in 2013, then showed up prominent blue and red emission wings in the first 2015's spectrum, which became even more prominent in the second 2015's spectrum (see Fig. 7).

The échelle spectrum of MN48 shows that the [Fe II] λ 7155 line has a flat-topped profile. This indicates that the line is formed in a region of constant expansion velocity and therefore its width is a measure of the terminal wind velocity, v_{∞} (Stahl et al. 1991). Using this line, we derived $v_{\infty}=152\pm 5 \text{ km s}^{-1}$. This figure is comparable to the wind velocity estimate of $\approx 200 \text{ km s}^{-1}$ based on the blue edge of the absorption component of the H α line (see Fig. 3).

The échelle spectrum also shows the prominent O I λ 7772–5 \AA triplet in absorption (Fig. 4), which is a good luminosity indicator (Merrill 1934). The EW of this triplet of $1.10\pm 0.02 \text{ \AA}$ (see Table 2) implies that MN48 is a B-type supergiant (e.g. Keenan & Hynek 1950). But unlike the normal

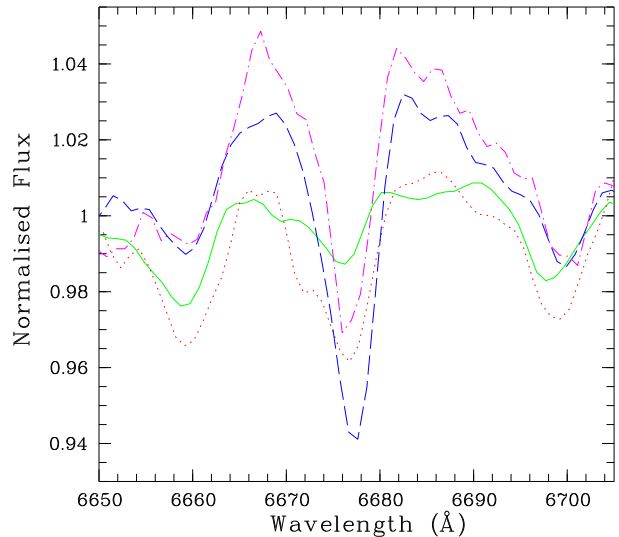


Figure 7. Evolution of the He I λ 6678 line profile with time: 2011 June 13 (solid green line), 2013 April 26 (dotted red line), 2015 May 4 (dashed blue line) and 2015 August 25 (dash-dotted magenta line).

blue supergiants of the same temperature, the wind of MN48 is slower (cf. Crowther 1997), which could be considered as an indication that this star is close to the Eddington limit (Groh, Hillier & Damiani 2011; Humphreys et al. 2014).

The [Fe II] λ 7155 line can also be used to estimate the systemic velocity of MN48 (Stahl et al. 2001). Using the échelle spectrum, we found a heliocentric RV of this line of $\approx -37 \text{ km s}^{-1}$. Interestingly, this RV is equal to the mean RV of other lines in the échelle spectrum (listed in Table 2), which are not affected by P Cygni absorption. We adopt this figure as a systemic velocity of MN48.

To summarize, the detected changes in the brightness and spectrum of MN48 imply that this star shows currently an S Dor activity and therefore it is one more (18th) example of the Galactic bona fide LBVs. A census of these objects is given in table 2 of Kniazev & Gvaramadze (2016).

4.2 Distance to and luminosity of MN48

The majority of LBVs are located beyond the confines of known star clusters and therefore they are likely runaway stars (Gvaramadze et al. 2012b). Just the isolation from other massive stars allows the LBVs to create coherent (observable) circumstellar nebulae, while within the parent clusters formation of nebulae is precluded because of the effect of stellar winds from neighbouring OB stars. On the other hand, the isolated location of the majority of LBVs makes their distances difficult to determine. Nonetheless, to get some idea on the distance to a particular isolated LBV, one can consider whether or not its luminosity would be reasonable if the star is placed in one or another spiral arm along the line of sight to it (cf. Gvaramadze et al. 2015b). Further constraint on the distance to an isolated LBV could be obtained from detection of its likely parent cluster.

To constrain the distance to (and hence the luminosity of) MN48, we note that the sightline towards this star first enters (e.g. Cordes & Lazio 2002) the Carina-Sagittarius

spiral arm (located at a distance of $d \sim 2$ kpc from the Sun), then (at $d \sim 3$ kpc) intersects the Crux-Scutum arm, and then twice crosses the Norma arm (at $d \sim 5$ and 12 kpc). The distances at which the sightline intersects the spiral arms correspond to distance modulus (DM) values of ≈ 11.5 , 12.4, 13.5 and 15.4 mag, respectively. To estimate the absolute visual magnitude, M_V , of MN48 for a given DM, one needs to know the visual extinction, A_V , towards this star.

To estimate A_V , we match the dereddened spectral slope of MN48 with those of stars of similar T_{eff} from the Stellar Spectral Flux Library by Pickles (1998). To estimate the temperature of MN48, we note that the 2015's spectra of this star are very similar to those of the classical LBV AG Car in 2003 January (see fig. 3 in Groh et al. 2009), when its T_{eff} was about 14000 K. Adopting this T_{eff} for MN48 and using the RSS spectra, we found the colour excess of $E(B - V) = 3.9 \pm 0.1$ mag⁵ and $A_V = 12.1 \pm 0.3$ mag (here we used the ratio of total to selective extinction of $R_V = 3.1$). With this A_V and $V = 15.7 \pm 0.5$ mag (see Table 3), and using the above values of DM, one finds, respectively, $M_V \approx -7.9 \pm 0.6$, -8.8 ± 0.6 , -9.9 ± 0.6 and -11.8 ± 0.6 mag. These absolute magnitudes translate to the luminosities of $\log(L_{\text{bol}}/L_{\odot}) \approx 5.5 \pm 0.2$, 5.9 ± 0.2 , 6.3 ± 0.2 and 7.1 ± 0.2 , respectively; here we assumed that the bolometric correction of MN48 is equal to that of AG Car in 2003 January (see above), i.e. ≈ -1.2 mag (Groh et al. 2009). One can see that the luminosity of MN48 would be unreasonably high if this star is located in the far segment of the Norma arm ($d = 12$ kpc) or further out. The other three luminosities are reasonable and imply that MN48 is located either on the S Dor instability strip or on the cool side of this strip (Wolf 1989; Groh et al. 2009) on the Hertzsprung-Russell diagram. Note that the high extinction towards MN48 argues against the short distance ($d \sim 2$ kpc) to this star, although this distance cannot completely be ruled out because a significant fraction of reddening of MN48 might be due to the dusty circumstellar material (cf. Gvaramadze et al. 2015b). We conclude, therefore, that it is likely that MN48 is located either in the Crux-Scutum arm or in the near segment of the Norma arm. In both cases, the luminosity of MN48 would exceed the Humphreys-Davidson luminosity limit (Humphreys & Davidson 1979) and the star would be subject to unsteady eruptive events.

The distance to MN48 could also be estimated through the systemic velocity of this star. This estimate, however, would be reasonable only if MN48 is not a runaway star with a significant peculiar radial velocity. Using R_V of MN48 of -37 km s⁻¹ and assuming the distance to the Galactic Centre of $R_0 = 8.0$ kpc and the circular rotation speed of the Galaxy of $\Theta_0 = 240$ km s⁻¹ (Reid et al. 2009), and the solar peculiar motion $(U_{\odot}, V_{\odot}, W_{\odot}) = (11.1, 12.2, 7.3)$ km s⁻¹ (Schönrich, Binney & Dehnen 2010), one finds the near and far kinematic distances to MN48 of ≈ 2.7 and 12.3 kpc. The former figure implies that MN48 is located in the interarm region, which would be possible only if this star is a high-velocity runaway moving almost along our line of sight (in this case, however, the kinematic distance estimate would be meaningless). At the latter distance, as noted above, the

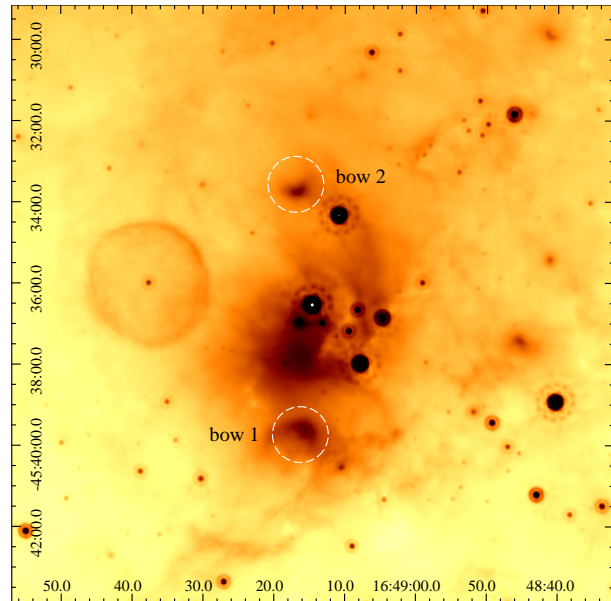


Figure 8. *Spitzer* MIPS 24 μ m image of MN48 and the H II region IRAS 16455–4531. The dashed circles mark two bow-shaped structures faced towards the centre of IRAS 16455–4531. The coordinates are in units of RA (J2000) and Dec. (J2000) on the horizontal and vertical scales, respectively. See text for details.

luminosity of MN48 would be unrealistically high. These considerations suggest that either the adopted systemic velocity of MN48 is incorrect or the star has a peculiar radial velocity, i.e. it is a runaway star (this possibility is further discussed in Sections 4.3 and 4.4).

4.3 MN48 and the H II region IRAS 16455–4531

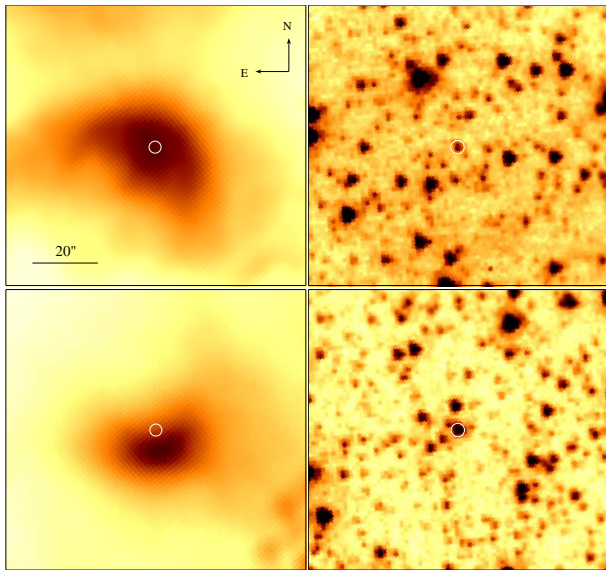
In Section 2, we mentioned that MN48 is located not far from the H II region IRAS 16455–4531 and that the enhanced brightness of the western edge of the nebula might be caused by the interaction of the nebula with the H II region. To discuss this possibility, we present in Fig. 8 the MIPS 24 μ m image of IRAS 16455–4531 and its close environment. On this image, besides MN48, one can see two bow-shaped structures (hereafter, bow 1 and bow 2) pointed towards the centre of the H II region. We interpret these structures as bow shocks produced because of interaction between a gas flow driven by a putative star cluster deeply embedded in the H II region and stellar winds of two (massive) stars in the halo of the cluster (cf. Povich et al. 2008). If our interpretation is correct, then the star cluster embedded in IRAS 16455–4531 might be the parent cluster to MN48 as well.

In Fig. 9 we show stars possibly associated with bow 1 and bow 2. These stars (hereafter, star 1 and star 2) are highly extinguished and visible only in the infrared. In Table 4, we give their coordinates and the *J* and *K* band photometry from the VISTA Variables in the Vía Láctea (VVV) survey Catalogue Data Release 1 (Saito et al. 2012). To produce the bow shocks, stars 1 and 2 should possess strong winds, i.e. they should be OB stars. In the absence of spectroscopic observations of stars 1 and 2, we will estimate their spectral

⁵ Note that this estimate only slightly depends on the adopted T_{eff} (Gvaramadze et al. 2012a).

Table 4. Details of two candidate bow-shock-producing stars around IRAS 16455–4531. See text for details.

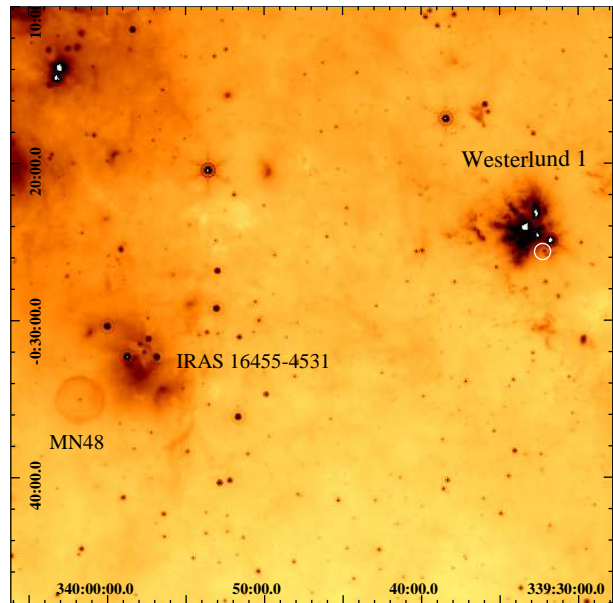
star	RA(J2000)	Dec.(J2000)	J (mag)	K (mag)	A_K (mag)	M_K (mag)	Spectral type
1	16 ^h 49 ^m 15 ^s .65	−45°39′35″.9	17.103±0.025	13.299±0.008	2.65	−2.84	B1 V
2	16 ^h 49 ^m 16 ^s .81	−45°33′39″.1	13.478±0.002	11.380±0.002	1.52	−3.63	O8 V


Figure 9. Left panels: MIPS 24 μm images of bow 1 (upper panel) and bow 2. Right panels: IRAC 3.6 μm images of the candidate bow-shock-producing stars (marked by white circles): star 1 (upper panel) and star 2. The orientation and the scale of the images are the same.

types by using their photometry and assuming that they are located at the same distance as IRAS 16455–4531.

The distance to IRAS 16455–4531 could be derived from RV of the strongest peak of the 6.668 GHz methanol maser emission from this H II region of -91 km s^{-1} (Walsh et al. 1995; Pestalozzi, Minier & Booth 2005). Using the same Galactic constants and the solar peculiar motion as in Section 4.2, one finds the near and far kinematic distances to IRAS 16455–4531 of ≈ 5.2 and 9.8 kpc. The former distance agrees with one of the two likely distances to MN48, which lends some support to the possibility that MN48 and IRAS 16455–4531 might be associated with each other. If so, then the difference in RVs of the both objects would imply that MN48 was ejected from its birth place with a radial velocity of $\approx 50 \text{ km s}^{-1}$.

Using the extinction law from Rieke & Lebofsky (1985), the photometric calibration of optical and infrared magnitudes for Galactic O stars by Martins & Plez (2006), and the J and K magnitudes from Table 4, we derived the K band extinction towards stars 1 and 2 of $A_K \approx 2.65$ and 1.52 mag, respectively. Then, assuming that both stars are located at 5 kpc, we derived their K band absolute magnitudes of -2.84 and -3.63 , which correspond to approximate spectral types of B1 V and O8 V, respectively. If subsequent spectroscopy of stars 1 and 2 will prove that they are indeed massive stars, then the idea that IRAS 16455–4531 might


Figure 10. *Spitzer* MIPS 24 μm image of MN48, the H II region IRAS 16455–4531 and the H II region associated with the young massive star cluster Westerlund 1. The position of the LBV W 243 is indicated by a white circle. The image is oriented with Galactic longitude (in units of degrees) increasing to the left and Galactic latitude decreasing upwards. See text for details.

be the birth place of MN48 would deserve more thorough consideration.

4.4 MN48 and the young massive star cluster Westerlund 1

It is also worthy of note that MN48 is located at only ≈ 0.5 degree from the young massive star cluster Westerlund 1 (see Fig. 10). This cluster contains dozens of massive stars (Clark et al. 2005), including the bona fide LBV W 243 (Clark & Negueruela 2004). Numerous distance estimates based on various methodologies place this cluster either in the Crux-Scutum arm (e.g. Kothes & Dougherty 2007; Koumpia & Bonanos 2012) or in the near segment of the Norma arm (e.g. Clark et al. 2005; Negueruela, Clark & Ritchie 2010), i.e. the cluster and MN48 could be at the same distance. The colour excess towards Westerlund 1 of $E(B - V) = 4.2 \pm 0.4$ mag (Negueruela et al. 2010) is comparable to that derived for MN48 in Section 4.2, which further strengthens the possibility that the distances to both objects are similar. Taken together, these make Westerlund 1 a good candidate for the parent cluster to MN48.

The large number of massive stars in the cluster and the high percentage of binaries among them (Ritchie et al. 2009), imply that Westerlund 1 was effective in producing runaway

stars through dynamical few-body encounters at early stages of the cluster evolution (Gvaramadze & Gualandris 2011; Fujii & Portegies Zwart 2011; Banerjee, Kroupa & Oh 2012). MN48 could be one of these stars. At a distance of 5 kpc, MN48 would be separated from Westerlund 1 by ≈ 44 pc in projection. This separation and the age of the cluster of ~ 5 Myr (Negueruela et al. 2010) imply a peculiar transverse velocity of MN48 of only about 10 km s^{-1} , provided that the star was ejected soon after the cluster formation. The actual ejection velocity could be higher if the star is moving close to our line of sight⁶ and/or if it was ejected because of a binary supernova explosion (in this case, the kinematic age of MN48 could be much smaller than the age of the cluster).

The existing proper motion measurements for MN48, however, are very unreliable, which did not allow us to check the possibility that this star was ejected from Westerlund 1. Hopefully, the space astrometry mission *Gaia* will provide proper motion and parallax measurements accurate enough to identify the parent cluster to MN48.

5 ACKNOWLEDGEMENTS

This work is supported by the Russian Foundation for Basic Research grant 16-02-00148. AYK also acknowledges support from the National Research Foundation (NRF) of South Africa. We thank Dave Kilkenny for getting for us V and I_c band images of MN48 with the SAAO 1-m telescope and the referee for useful comments. VVG. This research has made use of observations from the LCOGT network (programme SAO2015B-002), the NASA/IPAC Infrared Science Archive, which is operated by the Jet Propulsion Laboratory, California Institute of Technology, under contract with the National Aeronautics and Space Administration, the SIMBAD data base and the VizieR catalogue access tool, both operated at CDS, Strasbourg, France.

REFERENCES

Banerjee S., Kroupa P., Oh S., 2012, *ApJ*, 746, 15
 Ballester P., 1992, in Grosbol P.J., de Ruijsscher R.C.E., eds., 4th ESO/ST-ECF Data Analysis Workshop, ESO Conf. and Workshop Proc. Vol. 41, p. 177
 Barnes et al., 2008, in McLean I. S., Casali M. M., eds, Proc. SPIE Conf. Ser. Vol. 7014, Ground-based and Airborne Instrumentation for Astronomy II. SPIE, Bellingham, p. 70140K
 Berdnikov L. et al., 2012, *Astron. Rep.*, 56, 290
 Bramall D. G. et al., 2010, in McLean I. S., Ramsay S. K., Takami H., eds, Proc. SPIE Conf. Ser. Vol. 7735, Ground-based and Airborne Instrumentation for Astronomy III. SPIE, Bellingham, p. 77354F
 Bramall D. G. et al., 2010, in McLean I. S., Ramsay S. K., Takami H., eds, Proc. SPIE Conf. Ser. Vol. 8446, Ground-based and Airborne Instrumentation for Astronomy IV. SPIE, Bellingham, p. 84460A
 Brown T. M., et al., 2013, *PASP*, 125, 1031

Buckley D. A. H., Swart G. P., Meiring J. G., 2006, in Stepp L. M., ed., Proc. SPIE Conf. Ser. Vol. 6267, Ground-based and Airborne Telescopes. SPIE, Bellingham, p. 62670Z
 Burgh E. B., Nordsieck K. H., Kobulnicky H. A., Williams T. B., O'Donoghue D., Smith M. P., Percival J. W., 2003, in Iye M., Moorwood A. F. M., eds, Proc. SPIE Conf. Ser. Vol. 4841, Instrument Design and Performance for Optical/Infrared Ground-based Telescopes. SPIE, Bellingham, p. 1463
 Carey S. J. et al., 2009, *PASP*, 121, 76
 Clark J. S., Negueruela I., 2004, *A&A*, 413, L15
 Clark J. S., Negueruela I., Crowther P. A., Goodwin S. P., 2005, *A&A*, 434, 949
 Clark J. S., Egan M. P., Crowther P. A., Mizuno D. R., Larionov V. M., Arkharov A., 2003, *A&A*, 412, 185
 Conti P. S., 1984, in Maeder A., Renzini A., eds, Observational Tests of the Stellar Evolution Theory. Reidel, Dordrecht, p. 233
 Cordes J. M., Lazio T. J. W., 2002, astro-ph/0207156
 Crause L. A., et al., 2014, in Ramsay S. K., McLean I. S., Takami H., eds, Proc. SPIE Conf. Ser. Vol. 9147, Ground-based and Airborne Instrumentation for Astronomy V. SPIE, Bellingham, p. 91476T
 Crawford S. M. et al., 2010, in Silva D. R., Peck A. B., Soifer B. T., Proc. SPIE Conf. Ser. Vol. 7737, Observatory Operations: Strategies, Processes, and Systems III. SPIE, Bellingham, p. 773725
 Crowther P. A., 1997, in Nota A., Lamers H. J. G. L. M., eds, ASP Conf. Ser. Vol. 120, Luminous Blue Variables: Massive Stars in Transition. Astron. Soc. Pac., San Francisco, p. 51
 Cutri R. M. et al., 2003, 2Mass All Sky Catalog of point sources, VizieR Online Data Catalogue, 2246, 0
 Cutri R. M. et al., 2014, AllWISE Data Release, VizieR Online Data Catalogue, 2328, 0
 Egan M. P., Clark J. S., Mizuno D. R., Carey S. J., Steele I. A., Price S. D., 2002, *ApJ*, 572, 288
 Epchtein N. et al., 1999, *A&A*, 349, 236
 Fazio G. G. et al., 2004, *ApJS*, 154, 10
 Filippenko A.V., Barth A.J., Bower G.C., Ho L.C., Stringfellow G.S., Goodrich R.W., Porter A.C., 1995, *AJ*, 110, 2261
 Flagey N., Noriega-Crespo A., Billot N., Carey S. J., 2011, *ApJ*, 741, 4
 Flagey N., Noriega-Crespo A., Petric A. O., Geballe T. R., 2014, *AJ*, 148, 34
 Fujii M. S., Portegies Zwart S., 2011, *Science*, 334, 1380
 Gal-Yam A., Leonard D.C., 2009, *Nature*, 458, 865
 Groh J. H., Hillier D. J., Daminieli A., Whitelock P. A., Marang F., Rossi C., 2009, *ApJ*, 698, 1698
 Groh J. H., Hillier D. J., Daminieli A., 2011, *ApJ*, 736, 46
 Groh J. H., Meynet G., Ekström S., 2013, *A&A*, 550, L7
 Groh J. H., Meynet G., Georgy C., Ekström S., 2013, *A&A*, 558, A131
 Goodrich R.W., Stringfellow G.S., Penrod D.G., Filippenko A.V., 1989, *ApJ*, 342, 908
 Gvaramadze V. V., Gualandris A., 2011, *MNRAS*, 410, 304
 Gvaramadze V. V., Kniazev A. Y., Fabrika S., Sholukhova O., Berdnikov L. N., Cherepashchuk A. M., Zharova A. V., 2010a, *MNRAS*, 405, 520
 Gvaramadze V. V., Kniazev A. Y., Fabrika S., 2010b, *MNRAS*, 405, 1047

⁶ At the distances of 3.3 and 5 kpc, the systemic velocity of MN48 of -37 km s^{-1} corresponds to the peculiar radial velocity of 48 and 13 km s^{-1} , respectively.

- Gvaramadze V. V., Kniazev A. Y., Kroupa P., Oh S., 2011, *A&A*, 535, A29
- Gvaramadze V. V. et al., 2012a, *MNRAS*, 421, 3325
- Gvaramadze V. V., Weidner C., Kroupa P., Pflamm-Altenburg J., 2012b, *MNRAS*, 424, 3037
- Gvaramadze V. V., Kniazev A. Y., Berdnikov L. N., Langer N., Grebel E. K., Bestenlehner J. M., 2014, *MNRAS*, 445, L84
- Gvaramadze V. V. et al., 2015a, *MNRAS*, 454, 219
- Gvaramadze V. V., Kniazev A. Y., Berdnikov L. N., 2015b, *MNRAS*, 454, 3710
- Humphreys R. M., Davidson K., 1979, *ApJ*, 232, 409
- Humphreys R. M., Davidson K., 1994, *PASP*, 106, 1025
- Humphreys R. M., Weis K., Davidson K., Bomans D. J., Burggraf B., 2014, *ApJ*, 790, 48
- Keenan P. C., Hynek J. A., 1950, *ApJ*, 111, 1
- Kniazev A. Y., Pustilnik S. A., Grebel E. K., Lee H., Pramskij A. G., 2004, *ApJS*, 153, 429
- Kniazev A. Y. et al., 2008, *MNRAS*, 388, 1667
- Kniazev A. Y., Gvaramadze V. V., Berdnikov L. N., 2015, *MNRAS*, 449, L60
- Kniazev A. Y., Gvaramadze V. V., 2016, in proceedings of “SALT Science Conference 2015”, preprint (arXiv:1601.02849)
- Kobulnicky H. A., Nordsieck K. H., Burgh E. B., Smith M. P., Percival J. W., Williams T. B., O’Donoghue D., 2003, in Iye M., Moorwood A. F. M., eds, *Proc. SPIE Conf. Ser. Vol. 4841, Instrument Design and Performance for Optical/Infrared Ground-based Telescopes*. SPIE, Bellingham, p. 1634
- Koumpia E., Bonanos A. Z., 2012, *A&A*, 547, A30
- Kotak R., Vink J. S., 2006, *A&A*, 460, L5
- Kothes R., Dougherty, S. M., 2007, *A&A*, 468, 993
- Langer N., Hamann W.-R., Lennon M., Najarro F., Pauldrach A. W. A., Puls J., 1994, *A&A*, 290, 819
- Lennon D. J., Dufton P. L., Fitzsimmons A., 1993, *A&AS*, 97, 595
- Martins F., Plez B., 2006, *A&A*, 457, 637
- McLean B. J., Greene G. R., Lattanzi M. G., Pirenne B., 2000, in Manset N., Veillet C., Crabtree D., eds, *ASP Conf. Ser. Vol. 216, Astronomical Data Analysis Software and Systems IX*. Astron. Soc. Pac., San Francisco, p. 145
- Merrill P. W., 1934, *ApJ*, 79, 183
- Mizuno D. R. et al., 2010, *AJ*, 139, 1542
- Monet D. G. et al., 2003, *AJ*, 125, 984
- Negueruela I., Clark J. S., Ritchie B. W., 2010, *A&A*, 516, 78
- Nota A., Livio M., Clampin M., Schulte-Ladbeck R., 1995, *ApJ*, 448, 788
- Nowak M., Flagey N., Noriega-Crespo A., Billot N., Carey S. J., Paladini R., Van Dyk S. D., 2014, *ApJ*, 796, 116
- O’Donoghue D. et al., 2006, *MNRAS*, 372, 151
- Pestalozzi M. R., Minier V., Booth R. S., 2005, *A&A*, 432, 737
- Pickles A. J., 1998, *PASP*, 110, 863
- Povich M. S., Benjamin R. A., Whitney B. A., Babler B. L., Indebetouw R., Meade M. R., Churchwell E., 2008, *ApJ*, 689, 242
- Reid M. J., Menten K. M., Zheng X. W., Brunthaler A., Xu Y., 2009, *ApJ*, 705, 1548
- Rieke G. H., Lebofsky M. J., 1985, *ApJ*, 288, 618
- Rieke G. H. et al., 2004, *ApJS*, 154, 25
- Ritchie B. W., Clark J. S., Negueruela I., Crowther P. A., 2009, *A&A*, 507, 1585
- Saito R. K. et al., 2012, *A&A*, 537, A107
- Schönrich R., Binney J., Dehnen W., 2010, *MNRAS*, 403, 1829
- Skrutskie M. F. et al., 2006, *AJ*, 131, 1163
- Spitzer Science Center, 2009, *VizieR On-line Data Catalog*, 2293, 0
- Stahl O., Mandel H., Szeifert Th., Wolf B., Zhao F., 1991, *A&A*, 244, 467
- Stahl O., Mandel H., Wolf B., Gaeng Th., Kaufer A., Kneer R., Szeifert Th., Zhao F., 1993, *A&AS*, 99, 167
- Stahl O., Kaufer A., Tubbesing S., 1999, in Guenther, E. W., Stecklum, B., Klose, S., eds., *ASP Conf. Ser. Vol. 188, Optical and infrared spectroscopy of circumstellar matter*. Astron. Soc. Pac., San Francisco, p. 331
- Stahl O. et al., 2001, *A&A*, 375, 54
- Stothers R. B., Chin C.-W., 1996, *ApJ*, 468, 842
- Stringfellow G. S., Gvaramadze V. V., Beletsky Y., Kniazev A. Y., 2012a, in Richards M. T., Hubeny I., eds, *Proc. IAU Symp. 282, From Interacting Binaries to Exoplanets: Essential Modelling Tools*. Cambridge Univ. Press, Cambridge, p. 267
- Stringfellow G. S., Gvaramadze V. V., Beletsky Y., Kniazev A. Y., 2012b, in Drissen L., St-Louis N., Robert C., Moffat A. F. J., eds, *ASP Conf. Ser. Vol. 465, Four Decades of Massive Star Research – A Scientific Meeting in Honor of Anthony J. Moffat*. Astron. Soc. Pac., San Francisco, p. 514
- van Genderen A. M., 1982, *A&A*, 112, 61
- van Genderen A. M., 2001, *A&A*, 366, 508
- Wachter S., Mauerhan J. C., van Dyk S. D., Hoard D. W., Kafka S., Morris P. W., 2010, *AJ*, 139, 2330
- Wachter S., Mauerhan J., van Dyk S., Hoard D. W., Morris P., 2011, *Bull. Soc. R. Sci. Liège*, 80, 291
- Walborn N. R., 1980, *ApJS*, 44, 535
- Walsh A. J., Lyland A. R., Robinson G., Bourke T. L., James S. D., 1995, *PASA*, 12, 186
- Waters L. B. F. M., Izumiura H., Zaai P. A., Geballe T. R., Kester D. J. M., Bontekoe T. R., 1996, *A&A*, 313, 866
- Wolf B., 1989, *A&A*, 217, 87
- Wright E. L. et al., 2010, *AJ*, 140, 1868